Disrupting long-range polar order with an electric field

Hanzheng Guo, Xiaoming Liu, Fei Xue, Long-Qing Chen, Wei Hong, and Xiaoli Tan

Disrupting long-range polar order with an electric field

Hanzheng Guo[1,*], Xiaoming Liu[1], Fei Xue[2], Long-Qing Chen[2], Wei Hong[1,3] and Xiaoli Tan[1,*]

[1]*Department of Materials Science and Engineering, Iowa State University, Ames, IA 50011, USA*

[2]*Department of Materials Science and Engineering, The Pennsylvania State University, University Park, Pennsylvania, PA 16802, USA*

[3]*Department of Aerospace Engineering, Iowa State University, Ames, IA 50011, USA*

*Corresponding author. Email: ghanzheng@gmail.com; xtan@iastate.edu

Electric fields are known to favor long-range polar order through the aligning of electric dipoles in relation to Coulomb's force. Therefore, it would be surprising to observe a disordered polar state induced from an ordered state by electric fields. Here we show such an unusual phenomenon in a polycrystalline oxide where electric fields induce a ferroelectric to relaxor phase transition. The non-ergodic relaxor phase with disordered dipoles appears as an intermediate state under electric fields during polarization reversal of the ferroelectric phase. Using the phenomenological theory, the underlying mechanism for this unexpected behavior can be attributed to the slow kinetics of the ferroelectric to relaxor phase transition, as well as its competition against domain switching during electric reversal. The demonstrated material could also serve as a model system to study the transient stages in first-order phase transitions; the slow kinetics does not require the use of sophisticated ultrafast tools.

I. INTRODUCTION

Materials respond to physical forces (mechanical stress, electric fields, magnetic fields, temperature gradient, etc.) by adjusting their symmetries [1-3] and, if given the right conditions, transforming phases [4-10]. Many key engineering applications are based on these phase transitions, and the study of the transient states during a transition can provide invaluable information for condensed matter physics. But generally, these studies require advanced, ultrafast characterization tools owing to the momentary nature of the transient states [11,12].

It is commonly believed that an electric field favors long-range polar order by forcing the electric dipoles to align along the field direction. In the case of polycrystalline ferroelectric materials, that is, composed of randomly oriented grains and exhibiting spherical symmetry $\infty\infty m$, an electric field (with conical ∞m symmetry) always triggers an $\infty\infty m$ to ∞m symmetry change through aligning the ferroelectric domain polarization to the applied field direction [1]. This domain switching process yields remanence of macroscopic net polarization and imparts piezoelectricity to the ceramics [1]. Field reversal leads to the nucleation and growth of new domains with aligned polar vectors [13,14] preserving the ∞m macroscopic symmetry. This polarization reversal process has been extensively proven to occur in a fast manner, ranging between a few nanoseconds and several microseconds [15-18].

Such scenarios also apply to polycrystalline relaxor ferroelectrics in which a relaxor-to-ferroelectric state change is always favored under a sufficiently strong electric field through a first-order phase transition [19-21], yielding to a long-range ordered polarization arrangement [22-24]. In contrast to normal ferroelectrics, that is, the ferroelectric domains typically adopt uniform polarizations with long-range polar order on a macroscopic/mesoscopic scale, relaxors are of disordered nature due to the presence of randomly distributed polar nanoregions [23,25-

29]. Since there is a large number of polar nanodomains with disordered dipole moments in each individual grain, the $\infty\infty$m symmetry of a relaxor polycrystalline ceramic is even preserved down to the individual grain level. Coulomb forces exerted by electric field align the disordered dipoles and change the symmetry to ∞m, both at the grain level and at the whole specimen level, leading to a poled ferroelectric ceramic [19-23]. Electric fields would, therefore, favor only the poled ferroelectric phase with long-range polar order, which has been experimentally verified by a vast majority of studies so far [19-24].

Here we report that electric fields can induce a transition from a poled ferroelectric phase with long-range polar order to a relaxor phase with disordered dipoles. We reveal this unusual phase transition in a lead-free relaxor composition of $[(Bi_{1/2}Na_{1/2})_{0.95}Ba_{0.05}]_{0.98}La_{0.02}TiO_3$ (BNT-2La) in which a ferroelectric phase can be readily formed during electric poling [30,31]. The induced ferroelectric phase remains metastable upon field removal. When an electric field with reversed polarity is applied to this ferroelectric phase, the relaxor phase with nanodomains and disordered dipole moments is resumed. Our investigation suggests a relatively slow kinetics of the ferroelectric to relaxor phase transition, which competes against the ferroelectric domain polarization reversal process under a reversed field. Our findings provide critical information on the origin of excellent functional properties in perovskite oxides, such as piezoelectric and electrocaloric effects [32,33]. The present work also identifies a model material for studying first-order phase transitions that does not require ultrafast characterization tools to reveal the transient states.

II. EXPERIMENTAL PROCEDURE

The solid state reaction method was used to prepare the

$[(Bi_{1/2}Na_{1/2})_{0.95}Ba_{0.05}]_{0.98}La_{0.02}TiO_3$ (BNT-2La) polycrystalline ceramic, using Bi_2O_3 ($\geq$ 99.9%),

TiO_2 ($\geq$ 99.99%), La_2O_3 ($\geq$ 99.999%), Na_2CO_3 ($\geq$ 99.9%), and $BaCO_3$ ($\geq$ 99.997%) as starting

materials. Na_2CO_3 and La_2O_3 powders were baked before batching. The raw powders were

mixed in stoichiometric amounts and vibratory milled in ethanol with zirconia mill media for 6

hours. The mixture was dried and then calcined at 850 °C for 3 hours. With polyvinyl alcohol as

binder, the calcined powder was uniaxially pressed into circular disks under 300 MPa. Buried in

a protective powder of the same composition, the disks were sintered at 1150 ^{o}C for 3 hours in

alumina crucibles at a heating/cooling rate of 5 ^{o}C/min.

For dielectric, piezoelectric, and ferroelectric characterizations, silver films were

sputtered to serve as electrodes. The polarization (P) vs. electric field (E) hysteresis loops were

measured using a standardized ferroelectric test system (RT-66A, Radiant Technologies) at 4 Hz

and room temperature. The polarization current density (J) vs. electric field (E) curve was

determined by taking the derivative of polarization with respect to time, i.e., dP(t)/dt. The

longitudinal strain (x_{33}) developed under electric field in the form of a triangular wave of 0.05 Hz

was monitored with a MTI-2000 Fotonic Sensor (MTI Instruments Inc., Albany, NY). Dielectric

properties were measured using an LCR meter (HP-4284A, Hewlett-Packard) in a tube furnace at

a heating rate of 4 °C/min. For piezoelectricity measurements, the ceramic specimens were first

poled at 60 kV/cm for 20 minutes at room temperature (25 °C). Then, the poled sample was

subject to a DC field of 12 kV/cm with a reversed polarity for 1, 10, 30, and 60 minutes,

respectively. At each time interval, the piezoelectric coefficient d_{33} was measured with a piezo-

d_{33} meter (ZJ-4B, Institute of Acoustics, Chinese Academy of Sciences). Additional

measurements were also performed on the same sample at reverse DC fields of 9, 10, 11, 15, and 18 kV/cm.

For X-ray diffraction measurements, the same bulk sample as for d_{33} measurements was used. At each time interval under 12 kV/cm DC field, after d_{33} was measured, the silver film electrodes were removed using nitric acid dilute solution. The evolution of the ½(311) superlattice peak was immediately recorded on a Siemens D500 diffractometer using Cu-Kα radiation at a 0.02° step size and 150 s dwelling time per step. For electric field *in situ* TEM experiments, disk specimens (3 mm in diameter) were prepared from as-sintered pellets through standard procedures, including grinding, cutting, dimpling, and ion milling. The dimpled disks were annealed at 400 °C for 2 hours to minimize the residual stresses before Ar-ion milling to the point of electron transparency. *In situ* TEM experiments were carried out on a specimen that was crack-free at the edge of the central perforation on a Phillips CM30 microscope operated at 200 kV. Detailed experimental setup can be found in previous literature [6,21,31].

III. RESULTS AND DISCUSSION

A. Electric field-induced relaxor to ferroelectric transition.

We first illustrate the electric poling-induced relaxor to ferroelectric transition in a polycrystalline BNT-2La ceramic in Fig. 1. The virgin state ceramic is a non-ergodic relaxor at room temperature [30], as indicated by the strong frequency dispersion in the dielectric behavior (Fig. 1a) and representative nanometer-sized domains in its microstructures (Fig. 1b) revealed by transmission electron microscopy (TEM). Electron diffraction analysis (Fig. 1c) showed that ½{*ooo*}- and ½{*ooe*}-type (*o* and *e* stand for odd and even Miller indices, respectively)

superlattice spots [21,34,35] were present, indicating coexisting *R3c* and *P4bm* phases in the form of nanodomains [30]. Unlike the dynamically fluctuating polar nanoregions in ergodic relaxors [22,23], the static polar nanodomains shown in Fig. 1b can be irreversibly poled and aligned [31,36]. After poling at 60 kV/cm, a well-defined depolarization temperature T_d was observed in the dielectric curves (Fig. 1d). Correspondingly, lamellar domains with long-range polar orders were formed (Fig. 1e), and a *P4bm* to *R3c* symmetry change was also manifested by the disappearance of ½{*ooe*} superlattice spots and the significantly strengthened ½{*ooo*} spots (Fig. 1f). Both changes in the poled grain (Fig. 1e-1f) were metastable upon removal of the applied field. The evolution from nanodomains to lamellar domains demonstrated a relaxor to ferroelectric phase transition, which is a transition from disordered dipoles to long-range ordered dipoles; for a polycrystalline bulk specimen, it represents a transition from ∞∞m to ∞m symmetry.

B. Electric field-induced ferroelectric to relaxor transition.

For a better illustration, we show the evolution of polarization, *P*, and electrostrain, x_{33}, under the first cycle of a bipolar electric field of a virgin BNT-2La bulk sample in Fig. 2a. Correspondingly, the change of domain morphology and crystal structure under electric fields is monitored *in situ* in a [112]-aligned grain of a TEM specimen. In the virgin state (corresponding to Z_0 on the *P* and x_{33} curves), nanodomains were observed (Fig. 2b), as described earlier. Electron diffraction analysis confirmed the nature of the mixed *R3c* and *P4bm* phases (Fig. 2c). An increase in the electric field to Z_1 induced apparent macroscopic polarization but a negligible strain (Fig. 2a). Correspondingly, the applied field prompted the nucleation of lamellar domains along the {010} planes from the interior of the grain (Fig. 2d). Further increase in the field to Z_2 triggered an abrupt development of large polarization and strain (Fig. 2a), indicating that an

extensive relaxor to ferroelectric phase transition took place in the first quarter cycle of the applied field. On the microscopic scale, the nanodomains were consumed by long lamellar domains with walls along the {010} and {110} planes as well as by some large domains (Fig. 2e). The diffraction pattern shown in Fig. 2f indicates a single $R3c$ phase, suggesting a phase transition from $P4bm$ to $R3c$. In the second quarter cycle, when the field was removed (Z_3), large remanent polarization and remanent strain were recorded. At the same time, $R3c$ ferroelectric domains were observed to persist after removal of the electric field (Fig. 2g). These results are consistent with those shown in Fig. 1, indicating that the electric field favors the long-range polar order and transforms nanodomains into micron-sized domains.

The well-established ferroelectrics, e.g. $BaTiO_3$, $PbTiO_3$, $Pb(Zr,Ti)O_3$ and $BiFeO_3$, exhibit nucleation and growth of new domains with opposite polar vectors upon field reversal [13-18]. When they are in polycrystalline form, the ∞m macroscopic symmetry is presumably preserved during polarization reversal. However, this is not the case for the polycrystalline BNT-2La ceramic, where we observed an unusual ferroelectric to relaxor phase transition. With an increase in the magnitude of the applied field with reverse polarity in the third quarter cycle (point Z_5), the strain reached its minimum and the macroscopic polarization vanished (Fig. 2a). *In situ* TEM observation revealed a surprising recovery of nanodomains with short-range polar order (Fig. 2h) and a diffraction pattern almost identical to that of the virgin state (Fig. 2i). The weak ½{ooe} and ½{ooo} superlattice diffraction spots confirmed a return to the coexistence of $P4bm$ and $R3c$ phases in the form of nanodomains.

Such an unexpected disruption of the long-range polar order under the influence of an electric field was reproducibly observed, as shown in another grain in the same TEM specimen (Fig. 3). The nanodomains in the virgin state Z_0 (Fig. 3a) transformed into large lamellar

7

domains at Z_2 (Fig. 3c), with the major set of domain walls along the {010} planes. Although almost half the grain was under bend contours, the electron diffraction pattern (Fig. 3d) across the entire grain clearly suggests a phase transition from *P4bm* to *R3c*. The *R3c* lamellar domains remained mostly unchanged after the electric field was released (Z_3).

When the electric field reversed its polarity and reached Z_4, the majority of the lamellar domains were disrupted into nanodomains and only a few domains with {010} walls remained (Fig. 3e). Correlated to this morphology change was the reappearance of ½{*ooe*}-type superlattice diffraction spots and the weakening of the ½{*ooo*} spots (Fig. 3f). With an increase in the electric field to Z_5, the grain was dominated by nanodomains (Fig. 3g). The comparable intensities of the ½{*ooe*} and ½{*ooo*} superlattice spots in Fig. 3h suggest the coexistent *P4bm* and *R3c* phases in similar fractions. Again, the observations directly indicate that the electric field disrupts the long-range polar order and leads to a transition from ∞m to ∞∞m symmetry.

Further increase in the electric field from Z_5 to Z_8 reversed the macroscopic polarization and resumed the longitudinal strain (Fig. 2a). Correspondingly, the nanodomains coalesced and gradually grew into lamellar domains again (Fig. 3i-3k). The strengthening of the ½{*ooo*} superlattice spots and the absence of the ½{*ooe*} spots in the electron diffraction pattern (Fig. 3l) confirmed the reoccurrence of a *P4bm* to *R3c* phase transition. Based on these *in situ* TEM observations, we have demonstrated the complex phase transitions in the first and third quarter cycles of an applied electric field. The domain polarization reversal in the third quarter cycle took place through two transient phase transitions: from ferroelectric to relaxor and then from relaxor to ferroelectric, correspondingly accompanied with the disruption and re-formation of long-range polar order.

C. Verification in bulk samples.

We also note that these phase transitions leave signatures on the polarization vs. electric field hysteresis loop, which are easier to be seen on the curve of displacement current density, J, (Fig. 4a). The data represent measurements on the same bulk sample (as for data in Fig. 2a) for the second full cycle of electric field application. In contrast to a normal ferroelectric, which shows only one current density peak in the first and the third quarter cycles of bipolar fields [37], BNT-2La exhibited two anomalies in the first and the third quarter cycles. Based on our *in situ* TEM observations, peak J_1 corresponds to the ferroelectric to relaxor transition with the disruption of ferroelectric domains into nanodomains, while peak J_2 indicates the relaxor to ferroelectric transition with the coalescence and growth of nanodomains into large lamellar domains. The same processes were repeated at peaks J_3 and J_4.

We provide further verifications on a bulk sample with *ex situ* X-ray diffraction experiments. The evolution of the ½(311) superlattice diffraction peak was recorded, as well as the piezoelectric coefficient d_{33}. In the virgin state (Fig. 4b), the ½(311) peak was too weak to be detected by a conventional laboratory X-ray diffractometer. However, after poling at 60 kV/cm, the ½(311) peak appeared (marked "poled" in Fig. 4b), correlating very well with the TEM results of a single *R3c* ferroelectric phase. Simultaneously, piezoelectricity was developed after poling with a d_{33} value of ~147 pC/N, indicating the formation of long-range polar order. Subsequently, the sample was subjected to a DC field of -12 kV/cm (negative sign indicates a polarity opposite to the poling field). The ½(311) peak became weaker as time elapsed, and was nearly flattened out after 1 hour. Correspondingly, the d_{33} decayed and reached an almost zero value (Fig. 4d). During the time period under a DC field with a reversed polarity, the original relaxor phase was progressively resumed and a disruption of the long-range polar order took

9

place. Therefore, the X-ray diffraction measurements on the bulk sample not only verified the *in situ* TEM observations, but also revealed the very slow kinetics of the ferroelectric to relaxor phase transition.

The relaxation under a DC field with reversed polarity observed in the non-ergodic relaxor BNT-2La is analogous to the piezoelectric response decay in $Pb(Mg_{1/3}Nb_{2/3})O_3$-based ergodic relaxors after poling [24,38]. Both cases are attributed to the flipping of polar nanoregions aligned by the poling field to the initial disordered state. The stimulus in the ergodic relaxor case was solely thermal activation; however, for the non-ergodic relaxor presented here, the stimulus was primarily an electric field. We found the d_{33} reduction under a DC field with intensity in the range from -9 to -18 kV/cm (Fig. 4c-4d) could be well fitted with the Kohlrausch-Williams-Watt (KWW)-type relation [24,38]:

$$d_{33} = d_0 + d_1 \exp\left[-\left(\frac{t}{\tau}\right)^{\beta}\right] \qquad (1)$$

where d_0, d_1, and β are fitting parameters, τ is the characteristic time that describes the speed of relaxation. In the present case, τ represents a characteristic time for the recovery of the disordered state via the reverse ferroelectric to relaxor phase transition, which was found to be an exponential function of the field intensity (Fig. 4e). It is interesting to notice that the relaxation time τ varies by almost two orders of magnitude in the applied DC field range. Compared with other ferroelectric oxides, BNT-2La is clearly quite unique in the sense that its transient states during polarization reversal can be slowed down and easily manipulated. The transient relaxor state with disrupted dipole order can be induced out in a controllable manner over a timescale up to thousands of seconds.

D. Phenomenological modelling.

Generally speaking, an electric field as a driving force for phase transition is known to favor large ferroelectric domains with long-range polar order over disordered nanodomains, as exemplified previously in $(Bi_{1/2}Na_{1/2})TiO_3$-$BaTiO_3$ and $Pb(Mg_{1/3}Nb_{2/3})O_3$-based ceramics [19,21]. The electric field-assisted disruption of long-range polar order observed in the present work is highly unusual and seems contradictory to the common sense. Here, we will rationalize our observations using the following phenomenological theory [39]. The free energy density of the material in the ferroelectric phase and that in the relaxor phase are written as

$$W_{FE} = \frac{1}{2} a_{FE} P^2 + \frac{1}{4} b_{FE} P^4 \tag{2}$$

and

$$W_R = W_0 + \frac{1}{2} a_R P^2, \tag{3}$$

respectively, where a_{FE}, b_{FE}, and a_R are the coefficients for the Landau polynomial, and W_0 is the free energy of the relaxor phase in the ground state relative to that of the ferroelectric phase when $P = 0$. With $a_{FE} < 0$ and $b_{FE} > 0$, the free energy of the ferroelectric phase has double wells, as shown by Fig. 5a. Two energy minima can be identified at $P = \pm P^*$, where the spontaneous polarization $P^* = \sqrt{-a_{FE}/b_{FE}}$. The energy profile of the relaxor phase, on the other hand, has a single minimum at $P = 0$ (Fig. 5a). By referring to the initial part of the experimental P vs. E curve (e.g. segment Z_0-Z_1 on Fig. 2a), we extract the coefficient $a_R = 4\,\text{kV cm}/\mu C$ for the relaxor phase. The extraction of the parameters for the ferroelectric phase is difficult as a complete hysteresis loop in pure ferroelectric phase could not be achieved. However, they will be

selected later by considering the kinetic processes. Here the polynomials are expanded to the lowest order with the basic physics retained. While higher order energy functions may provide better fitting to the experiments, such a practice is not the point of interest of the current article.

By further assuming the rule of mixture between the two phases, we write the total free energy density, including the energy contribution from the external electric field E as

$$G = (1 - f_R)W_{FE} + f_R W_R - EP, \qquad (4)$$

with f_R being the volume fraction of the relaxor phase. From the experimental results, especially that of the relaxation tests under a reverse DC field, it is evident that under zero or low electric field the relaxor phase is thermodynamically stable while the ferroelectric phase is metastable: $W_0 < W_{FE}(P^*) = -a_{FE}^2/4b_{FE}$. A reasonable value for W_0 is taken as -700 mJ/cm^3, which will give the critical electric fields for the phase transitions close to experimental values. Despite the lower free energy, the energy barrier retards the transition between the two phases. When the applied electric field on the BNT-2La polycrystalline sample reverses its polarity and increases in amplitude, at least two kinetic processes take place: 180° polarization reversal while remaining in the ferroelectric phase, and the ferroelectric to relaxor phase transition. When the reversed electric field is further increased beyond a critical value, the relaxor phase transforms back to the energetically more favorable ferroelectric phase with reversed polarizations. For a polycrystalline BNT-2La, the two processes may take place simultaneously, but have distinct rate dependencies. It is believed that the domain switching is relatively fast [15-18] while the phase transition is relatively slow and thus dependent on the loading rate [40,41]. As a result, the intermediate relaxor phase during polarization reversal is only seen under relatively slow loading conditions.

Inspired by the KWW-type relaxation behavior, Eq. (1), we model the rate of change of the volume fraction of the ferroelectric phase in the positive polar state, f_+, under constant electric field, as:

$$\frac{df_+}{dt} = -\frac{\beta}{\tau^\beta (t-t_0)^{1-\beta}} f_+ .$$ (5)

Here, parameters τ and β are the same as those in Eq. (1), and t_0 is the onset of relaxation, i.e. the time when the field is applied. As shown in Fig. 4c-4e, both the characteristic time τ and the stretching exponent β are functions of the applied electric field E. Under a constant applied field, the integration of Eq. (5) recovers the KWW-type relaxation, Eq. (1). Under a varying electric field, however, Eq. (5) cannot be directly applied, as there is no set time t_0 for the entire process. Following the usual approach in modeling viscoelastic materials, we consider the continuously changing electric field as the superposition of numerous infinitesimal steps, the response of which can be captured by Eq. (5). If we rewrite Eq. (5) in the form $df_+/dt = -g\, f_+/(t-t_0)^{1-\beta}$, the accumulative relaxation behavior can then be represented by

$$\frac{df_+}{dt} = -\left[\frac{g(0)}{t^{1-\beta}} + \int_0^t \frac{\dot{g}(t_0)}{(t-t_0)^{1-\beta}} dt_0 \right] f_+ ,$$ (6)

where $g = \beta/\tau^\beta$, and $\dot{g}$ is its time derivative. Here for simplicity, we will take β to be a constant $\beta = 0.25$, and extract τ from Fig. 4e by fitting it to an exponential function

$$\tau(E) = \tau_0 \exp\left(\frac{E}{E_0} \right),$$ (7)

13

with $\tau_0 \approx 3.2 \times 10^5 \, \text{s}$ and $E_0 \approx 2 \, \text{kV} / \text{cm}$.

For simplicity, we assume the same kinetics for the relaxor to ferroelectric phase transition

$$\frac{df_R}{dt} = -\left[\frac{h(0)}{t^{1-\beta}} + \int_0^t \frac{\dot{h}(t_0)}{(t-t_0)^{1-\beta}} dt_0 \right] f_R, \tag{8}$$

where $h = \beta / \tau'^\beta$. The characteristic time is assumed to have the same exponential dependence on the applied field E but with an offset ΔE: $\tau' = \tau_0 \exp[(E + \Delta E)/E_0]$. The offset is taken to be the field difference between the two characteristic peaks (J_3 and J_4) of the current density curve in Fig. 4a, $\Delta E \approx 25 \, \text{kV} / \text{cm}$.

Now let us turn to the kinetics of the polarization reversal in the ferroelectric phase. It is assumed that the polarization reversal is much faster than the loading rate, so that the process may be regarded as rate-independent. To represent the rate-independent kinetics of the polarization reversal process, we assume the coercive field of the ferroelectric phase, $E_c = -\frac{2}{3} a_{FE} P^*$, to be a random variable following Gaussian distribution with mean value $\overline{E}_c$ and standard deviation σ_E. To arrive at a hysteresis loop similar to that observed in experiments, the mean coercive field is taken to be between the forward and reverse ferroelectric $\leftrightarrow$ relaxor phase transitions, $\overline{E}_c \approx 45 \, \text{kV/cm}$, and a standard deviation $\sigma_E \approx 4 \, \text{kV/cm}$ is also taken. The parameters for the free energy Eq. (2) are selected by taking a constant value $b_{FE} = 0.004 \, \text{kVcm}^5 / \mu\text{C}^3$, and keep a_{FE} as a random value to match the distribution of E_c.

Under a reverse field E, the grains with $E_c < E$ will undergo polarization reversal, while those with $E_c > E$ remains in the original polar state. The rate of change in the volume fraction f_+ due to polarization reversal is thus

$$\frac{df_+}{dt} = \frac{e^{-\left(\frac{E+\bar{E}_c}{2\sigma_E}\right)^2}}{\sigma_E \sqrt{2\pi}} \frac{dE}{dt} f_+ . \qquad (9)$$

Here, we further assume that the two kinetic processes act independently and do not interact with each other. Summing over the contributions from the two kinetic processes, we obtain the rate of change in the volume fractions of the positive and negative polar states

$$\frac{df_+}{dt} = -\left[\frac{g(0)}{t^{1-\beta}} + \int_0^t \frac{\dot{g}(t_0)}{(t-t_0)^{1-\beta}} dt_0 - \frac{e^{-\left(\frac{E+\bar{E}_c}{2\sigma_E}\right)^2}}{\sigma_E \sqrt{2\pi}} \frac{dE}{dt}\right] f_+ . \qquad (10)$$

$$\frac{df_-}{dt} = \left[\frac{h(0)}{t^{1-\beta}} + \int_0^t \frac{\dot{h}(t_0)}{(t-t_0)^{1-\beta}} dt_0\right] f_R - \frac{e^{-\left(\frac{E+\bar{E}_c}{2\sigma_E}\right)^2}}{\sigma_E \sqrt{2\pi}} \frac{dE}{dt} f_+ . \qquad (11)$$

These equations can be applied to the upper branch of the *P-E* hysteresis loop when the applied field decreases from the positive peak value. A similar set of equations can be prescribed when the field increases from the negative polarity. The electric field dependence of τ on the lower branch of the hysteresis loop, however, will need to be adjusted accordingly by changing the sign of the electric field.

Upon integration of Eqs. (10) and (11) simultaneously, the evolution of the volume fractions $f_+(t)$ and $f_-(t)$ can be computed. The volume fraction of the relaxor phase is simply

given by $f_R = 1 - f_+ - f_-$ (Fig. 5b). Subsequently, the resultant polarization can be evaluated by using the rule of mixture

$$P = f_+ P_+ + f_- P_- + f_R P_R , \tag{12}$$

where P_+, P_-, and P_R are the polarization of the corresponding phases under the same electric field, given by Eqs. (2) and (3).

The numerical result at a frequency of 4 Hz is plotted in Fig. 5c, together with the response of the pure ferroelectric phase and the pure relaxor phase. In Fig. 5c, all the key features on the experimentally measured *P-E* curve (Fig. 4a) are reproduced. Particularly, the two drops of polarization in the first and the third quarter cycles of applied field are observed, which correspond to peaks J_1 and J_2, and J_3 and J_4 in Fig. 4a, respectively. Under slow loading rate, the required electric field of the phase transition is smaller than that of polarization reversal. Therefore, in some regions, the polarization reversal is completed through two phase transitions, instead of pure flipping of the polarization vectors.

IV. CONCLUSIONS

In summary, an electric field-induced disruption of long-range polar order in a lead-free perovskite oxide was directly observed using *in situ* TEM. Dielectric, ferroelectric, electromechanical (strain and piezoelectric coefficient), as well as X-ray diffraction measurements on bulk polycrystalline samples supported the TEM results and further suggested that this unusual phenomenon represents a ferroelectric to relaxor phase transition. Even though the experimental observations seem to violate Coulomb's Law, it can be rationalized by a phenomenological model which takes the large difference in kinetics between the phase

16

transition and the polarization reversal processes into account. The proposed kinetics model reveals the change in volume fractions of various phases during polarization reversal and reproduces the experimentally measured P vs. E hysteresis loop.

Reference

[1] R.E. Newnham, *Properties of materials - anisotropy, symmetry, structure*, Oxford University Press, New York, 2005.

[2] M. Håkansson, T. Löfwander, and M. Fogelström, Nature Phys. **11**, 755 (2015).

[3] A. Biancoli, C.M. Fancher, J.L. Jones, and D. Damjanovic, Nature Mater. **14**, 224 (2015).

[4] K. Binder, Rep. Prog. Phys. **50**, 783 (1987).

[5] D.S. Fisher, M.P.A. Fisher, and D.A. Huse, Phys. Rev. B **43**, 130 (1991).

[6] H. Guo, B.K. Voas, S. Zhang, C. Zhou, X. Ren, S.P. Beckman, and X. Tan, Phys. Rev. B **90**, 100104 (2014).

[7] R. Kainuma, Y. Imano, W. Ito, Y. Sutou, H. Morito, S. Okamoto, O. Kitakami, K. Oikawa, A. Fujita, T. Kanomata, and K. Ishida, Nature **439**, 957 (2006).

[8] T. Matsuoka and K. Shimizu, Nature **458**, 186 (2009).

[9] D. Ehre, E. Lavert, M. Lahav, and I. Lubomirsky, Science **327**, 672 (2010).

[10] D. Chiba, S. Fukami, K. Shimamura, N. Ishiwata, K. Kobayashi, and T. Ono, Nat. Mater. **10**, 853 (2011).

[11] C. Rose-Petruck, R. Jimenez, T. Guo, A. Cavaller, C.W. Siders, F. Rksi, J.A. Squier, B.C. Walker, K.R. Wilson, and C.P.J. Barty, Nature **398**, 310 (1999).

[12] A.H. Zewail, Science **328**, 187 (2010).

[13] W.J. Merz, Phys. Rev. **95**, 690 (1954).

[14] Y.H. Shin, I. Grinberg, I.W. Chen, and A.M. Rappe, Nature **449**, 881 (2007).

[15] N. Balke, M. Gajek, A.K. Tagantsev, L.W. Martin, Y.-H. Chu, R. Ramesh, and S.V. Kalinin, Adv. Funct. Mater. **20**, 3466 (2010).

[16] A. Gruverman, D. Wu, and J.F. Scott, Phys. Rev. Lett. **100**, 097601 (2008).

[17] S.M. Yang, T.H. Kim, J.-G. Yoon, and T.W. Noh, Adv. Funct. Mater. **22**, 2310 (2012).

[18] Y. Kim, X. Lu, S. Jesse, D. Hesse, M. Alexe, and S.V. Kalinin, Adv. Funct. Mater. **23**, 3971 (2013).

[19] W. Qu, X. Zhao, and X. Tan, J. Appl. Phys. **102**, 084101 (2007).

[20] J.E. Daniels, W. Jo, J. Rödel, and J.L. Jones, Appl. Phys. Lett. **95**, 032904 (2009).

[21] C. Ma, H. Guo, S.P. Beckman, and X. Tan, Phys. Rev. Lett.**109**, 107602 (2012).

[22] L.E. Cross, Ferroelectrics **76**, 241 (1987).

[23] A.A. Bokov and Z.-G. Ye, J. Mater. Sci. **41**, 31 (2006).

[24] V.V. Shvartsman, B. Dkhil, and A.L. Kholkin, Annu. Rev. Mater. Res. **43**, 423 (2013).

[25] N. De Mathan, E. Husson, G. Calvarn, J.R. Gavarri, A.W. Hewat, and A. Morell, J. Phys. Condens. Matter **3**, 8159 (1991).

[26] W. Westphal, W. Kleemann, and M.D. Glinchuk, Phys. Rev. Lett. **68**, 847 (1992).

[27] D. Viehland, S.J. Jang, L.E. Cross, and M. Wuttig, Phys. Rev. B **46**, 8003 (1992).

[28] B.P. Burton, E. Cockayne, and U.V. Waghmare, Phys. Rev. B **72**, 064113 (2005).

[29] G.Y. Xu, Z. Zhong, Y. Bing, Z.-G. Ye, and G. Shirane, Nat. Mater. **5**, 134 (2006).

[30] X. Liu, H. Guo, and X. Tan, J. Eur. Ceram. Soc. **34**, 2997 (2014).

[31] H. Guo, X. Liu, and X. Tan, Adv. Funct. Mater. **25**, 270 (2015).

[32] S.E. Park and T.R. Shrout, J. Appl. Phys. **82**, 1804 (1997).

[33] G. Schmidt, H. Arndt, G. Borchhardt, J. von Cieminski, T. Petzsche, K. Borman, A. Sternberg, A. Zimite, and V.A. Isupov, Phys. Stat. Sol. (a) **63**, 501 (1981).

[34] A.M. Glazer, Acta Cryst. A **31**, 756 (1975).

[35] D.I. Woodward and M. Reaney, Acta Cryst. B **61**, 387 (2005).

[36] H. Guo, C. Ma, X. Liu, and X. Tan, Appl. Phys. Lett. **102**, 092902 (2013).

[37] L. Jin, F. Li, and S.J. Zhang, J. Am. Ceram. Soc. **97**, 1 (2014).

[38] S.V. Kalinin, B.J. Rodriguez, J.D. Budai, S. Jesse, A.N. Morozovska, A.A. Bokov, and Z.-G. Ye, Phys. Rev. B **81**, 064107 (2010).

[39] A.F. Devonshire, Phil. Mag. **40**, 1040 (1949).

[40] Y. Xu, W. Hong, Y. Feng, and X. Tan, Appl. Phys. Lett. **104**, 052903 (2014).

[41] H. Guo and X. Tan, Phys. Rev. B **91**, 144104 (2015).
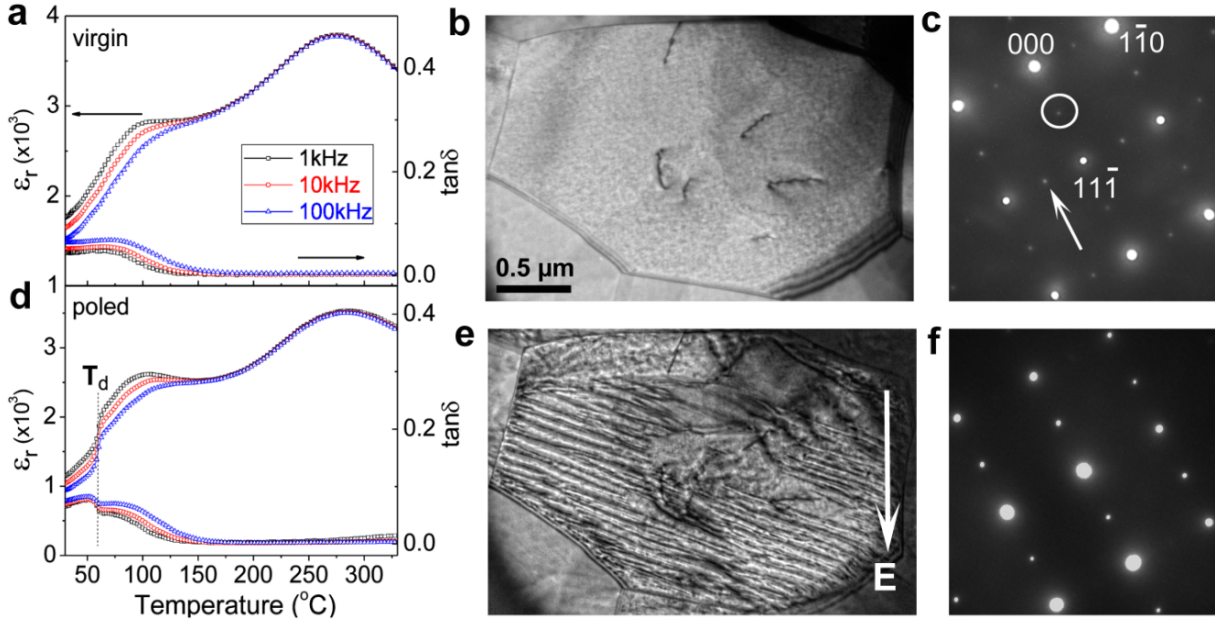
FIG. 1 The relaxor to ferroelectric transition during electric poling in BNT-2La demonstrated by dielectric behavior and *in situ* TEM observations. (a) Temperature dependent dielectric constant and loss tangent for a virgin bulk sample. (b) Bright field micrograph of a grain along its [112] zone axis, and (c) the corresponding electron diffraction pattern prior to poling. (d) Temperature dependent dielectric properties of the same bulk sample as in (a) after poling. (e) Bright field micrograph and (f) electron diffraction pattern of the same grain as in (b) after poling. The apparent depolarization temperature T_d is marked in (d). The nominal direction of the poling field in the *in situ* TEM experiment is indicated by the bright arrow in (e). The ½{*ooo*} and ½{*ooe*} superlattice diffraction spots are highlighted by a bright circle and a bright arrow, respectively, in (c).
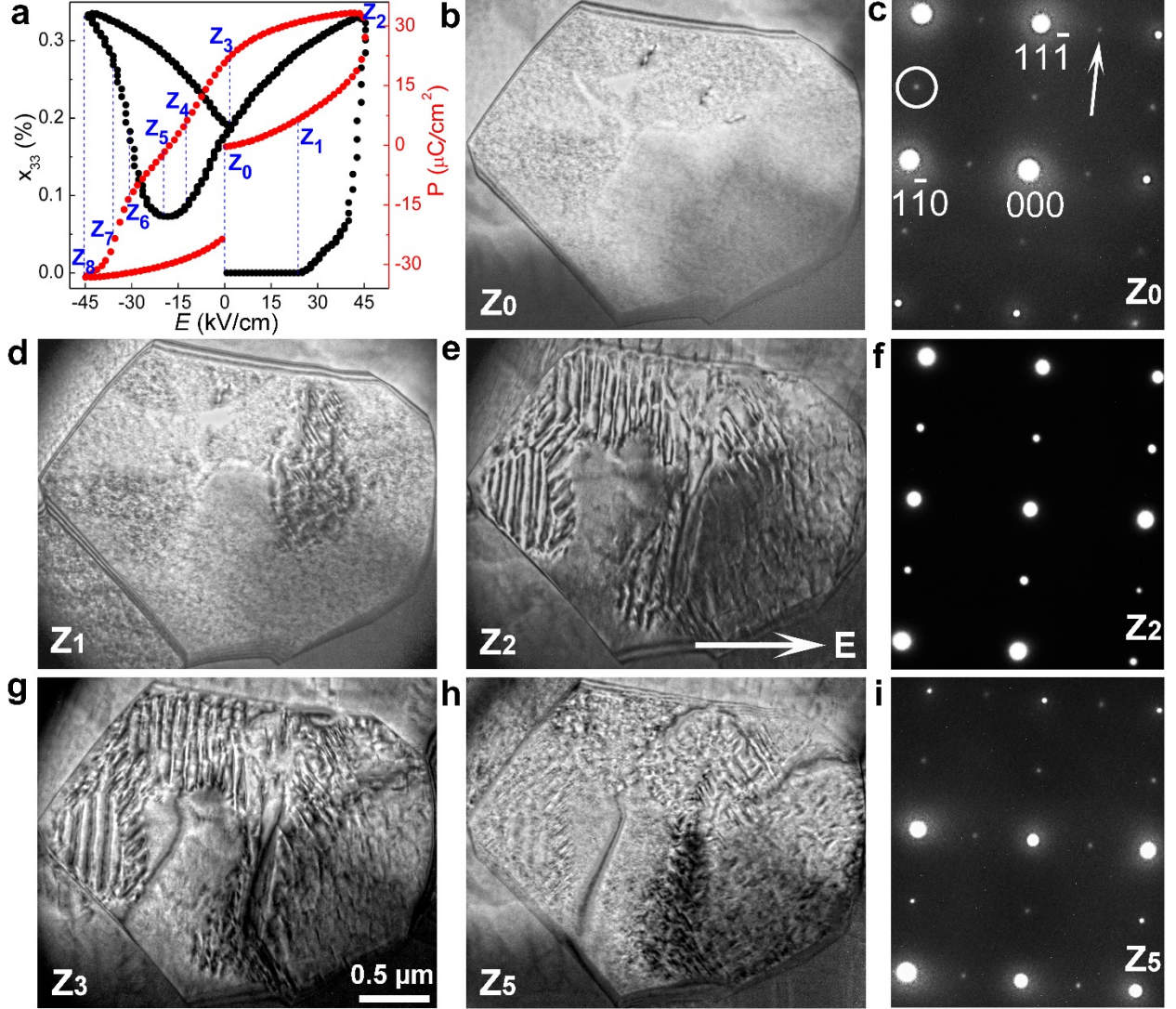
FIG. 2 Development and disruption of long-range polar order in BNT-2La. (a) Polarization, P, and longitudinal strain, x_{33}, developed under applied field of a bulk sample. The point pairs on the polarization and strain curves marked as Z_0 through Z_8 indicate the fields where corresponding *in situ* TEM observations were recorded. (b)-(i) The corresponding *in situ* TEM results on a [112]-aligned grain. The positive direction of applied fields in the TEM experiment is indicated by the bright arrow in (e). The ½{ooo} and ½{ooe} superlattice diffraction spots are highlighted by a bright circle and a bright arrow, respectively, in (c).
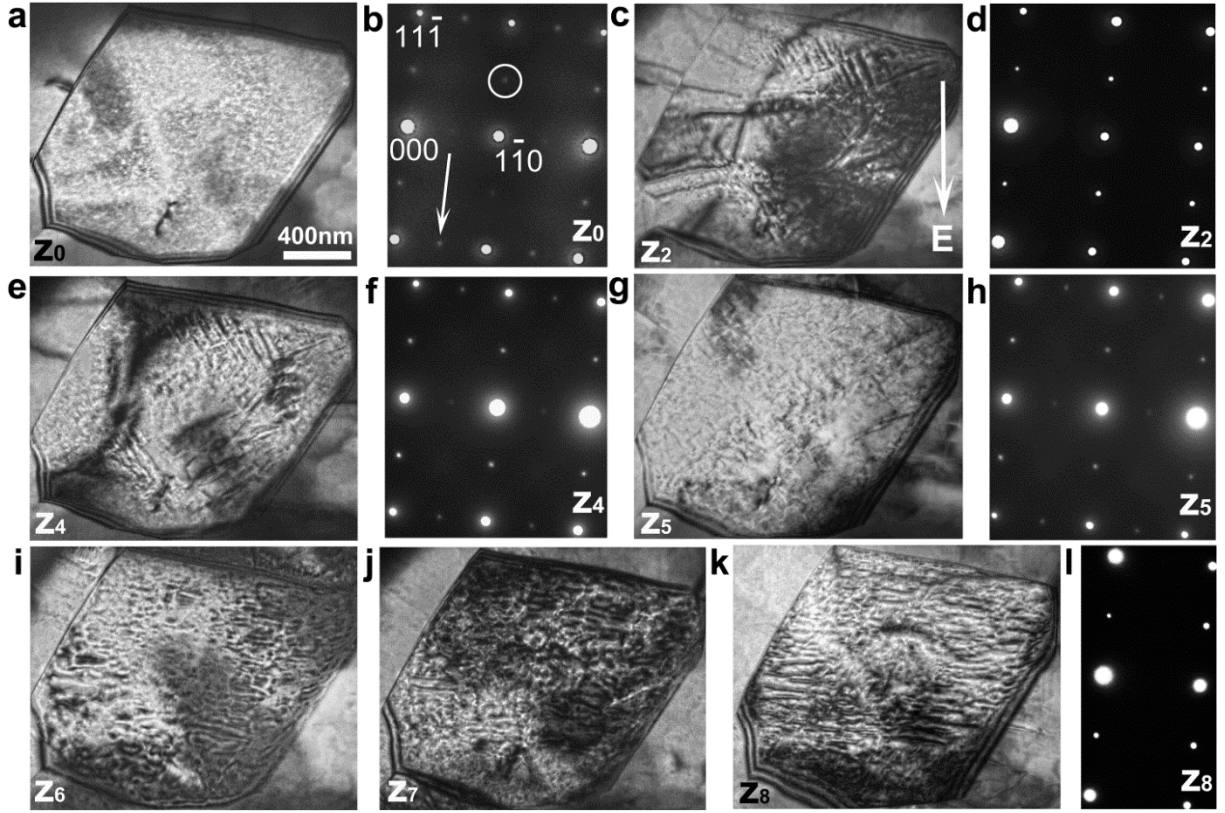
FIG. 3 *In situ* TEM observations on another [112]-aligned grain in the same TEM specimen as in Fig. 2. The positive direction of the applied field is indicated by the bright arrow in (c) and Z_0, Z_2, Z_4, Z_5, Z_6, Z_7, Z_8 mark the corresponding fields indicated in Fig. 2a. The ½{ooo} and ½{ooe} superlattice diffraction spots are highlighted by a bright circle and a bright arrow, respectively, in (b).
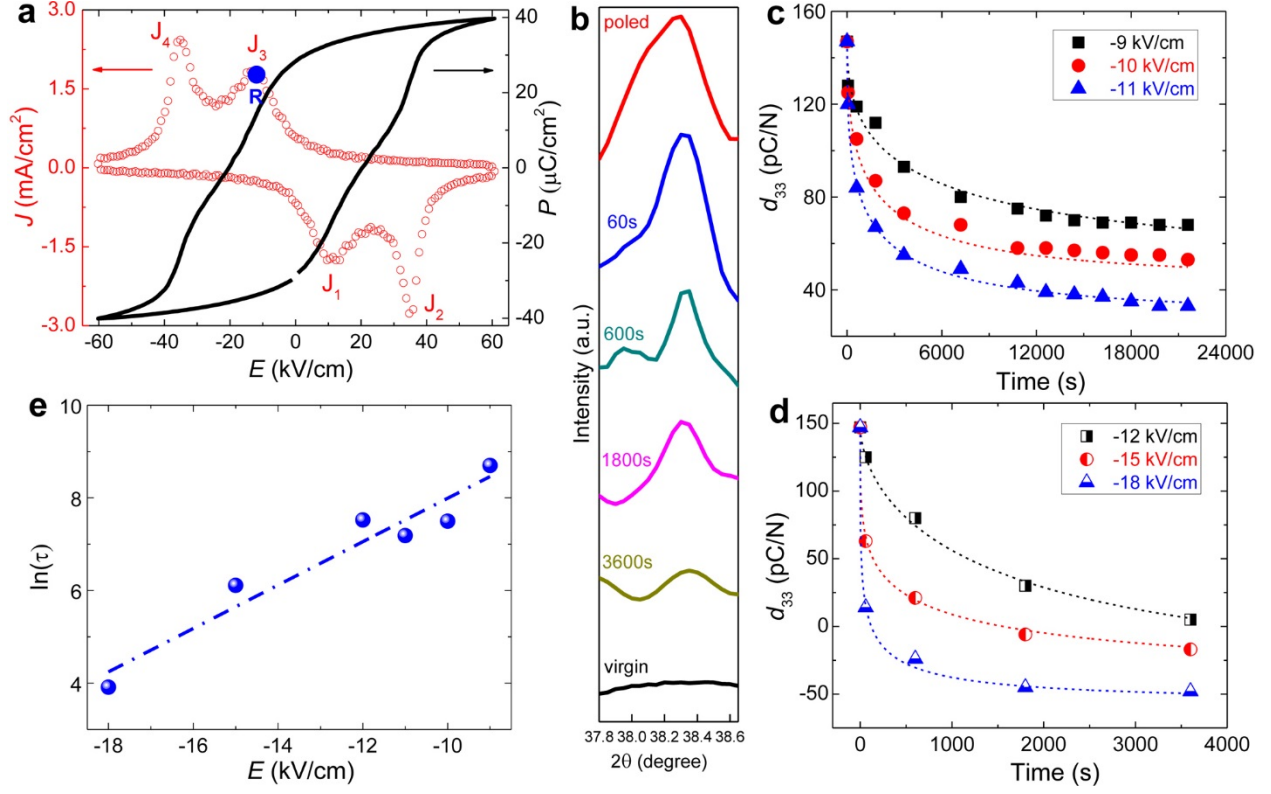
FIG. 4 Disrupting long-range polar order by electric field demonstrated in a bulk BNT-2La polycrystalline sample. (a) Polarization, P, vs. electric field, E, hysteresis loop during the second cycle of the bipolar electric field. The corresponding polarization current density, J, curve reveals two anomalies in both the first and the third quarter cycle. (b) Evolution of the ½(311) superlattice diffraction peak monitored by X-ray diffraction on a disk sample first poled at 60 kV/cm for 20 minutes (marked as "poled"), and then subjected to a DC field of -12 kV/cm (corresponding to the condition marked as "R" in (a)) for various times. The reduction in d_{33} of a poled BNT-2La sample under a series of reverse DC electric fields are shown in (c) for electric fields of -9, -10, and -11 kV/cm, and (d) for electric fields of -12, -15, and -18 kV/cm. Experimentally measured d_{33} after each time period are shown as discrete points, while the dashed lines are fitting curves derived using the KWW relationship. Error

bars for d_{33} are of the order of the size of symbols and not shown. (e) Correlation of the characteristic time τ with the amplitude of the reverse DC field.
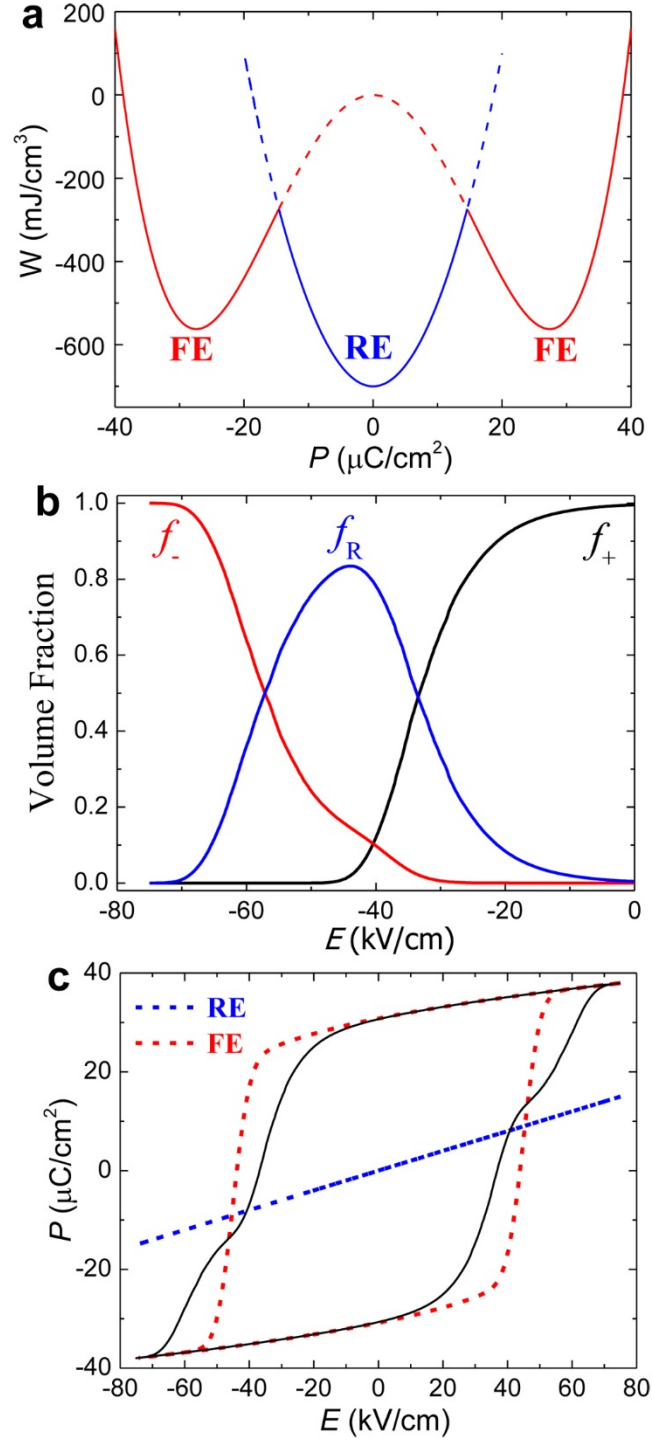
FIG. 5 Rationalization of the electric field-induced ferroelectric to relaxor transition in

polycrystalline BNT-2La with the phenomenological model. (a) The free energy density

profile of the ferroelectric phase (red) and the relaxor phase (blue) of BNT-2La at room

temperature. The phase transition path marked by the arrows shows a lower energy barrier

than polarization reversal and corresponds to the J_3 and J_4 peaks in Fig. 4a. (b) The change in

the volume fractions of various phases during polarization reversal in the third quarter cycle

of electric field. f_R, the volume fraction of the relaxor phase; f_+ and f_-, the volume fraction of

the ferroelectric phase in the positive and the negative polar state, respectively. (c) Calculated

P vs. E hysteresis loop with mixed phases (black curve), plotted together with the constituent

ferroelectric (red) and relaxor (blue) phases. FE and RE stand for ferroelectric and relaxor,

respectively.